Supplementary material for the article:

Wang, L.; Zlatar, M.; Vlahović, F.; Demeshko, S.; Philouze, C.; Molton, F.; Gennari, M.; Meyer, F.; Duboc, C.; Gruden, M. Experimental and Theoretical Identification of the Origin of Magnetic Anisotropy in Intermediate Spin Iron(III) Complexes. *Chemistry - A European Journal* **2018**, *24* (20), 5091–5094. https://doi.org/10.1002/chem.201705989

CHEMISTRY
A European Journal

Supporting Information

Experimental and Theoretical Identification of the Origin of Magnetic Anisotropy in Intermediate Spin Iron(III) Complexes

Lianke Wang,[a] Matija Zlatar,[b] Filip Vlahović,[c] Serhiy Demeshko,[d] Christian Philouze,[a] Florian Molton,[a] Marcello Gennari,[a] Franc Meyer,[d] Carole Duboc,*[a] and Maja Gruden*[c]

chem_201705989_sm_miscellaneous_information.pdf

Supplementary material

S1. Crystallographic data.

Crystallographic data for **Fe(L)Br** (CCDC 1811373) and **Fe(L)I** (CCDC number 1579777) are given in Table S1.1 and selected bond lengths and angles for **Fe(L)X** (X=Cl, Br, I) in Tables S1.2. Single-crystal diffraction data were measured on a Bruker-AXS-Enraf-Nonius Kappa diffractometer with an APEXII area detector and an Incoatec high brilliance microfocus source (MoKα radiation, Multilayers mirrors monochromator, λ 0.71073Å) at 200 K. The OLEX2 program package was used for cell refinements and data reductions. An absorption correction (SADABS) was applied to the data. Molecular structures were solved by charge flipping and refined on F2 by full matrix least-squares techniques, using the SHELXTL package. All non-hydrogen atoms were refined anisotropically and all hydrogen atoms were placed at their calculated positions.

Table S1. Crystallographic Data for **Fe(L)Br and Fe(L)I**.

	Fe(L)I	**Fe(L)Br**
empirical formula	$C_{38}H_{30}FeIN_2S_2$	$C_{38}H_{30}BrFeN_2S_2$
formula weight	761.51	714.52
crystal system	monoclinic	monoclinic
space group	P 21/c	P 21/c
a Å	14.510(3)	14.442(3)
b Å	15.233(3)	15.102(3)
c Å	16.097(3)	16.044(3)
α °	90	90
β °	112.79(3)	113.51(3)
γ °	90	90
V Å^3	3280.2(13)	3208.7(13)
Z	4	4
T K	200	200.0
D_{calcd} g·cm^{-3}	1.542	1.479
μ mm^{-1}	1.558	1.876
θ range °	2.090-29.997	2.098-25.000
total no. data	32934	32515
no.unique data	9513	5559
no. params refined	397	397
R_1	0.0401	0.0523
wR_2	0.0909	0.1448
GOF	1.098	1.106

Table S2. Selected bond lengths (Å) and angles (°) for **Fe(L)X** (X= I, Br, Cl).

Fe(L)Cl[a]		**Fe(L)Br**		**Fe(L)I**	
Cl1-Fe1	2.3130(10)	Br1-Fe1	2.4730(11)	I1-Fe1	2.6726(11)
Fe1-S1	2.2183(7)	Fe1-S2	2.2156(14)	Fe1-S1	2.2062(9)
Fe1-S2	2.2312(7)	Fe1-S1	2.2243(13)	Fe1-S2	2.2107(9)
Fe1-N2	2.0314(18)	Fe1-N2	2.058(4)	Fe1-N2	2.029(2)
Fe1-N1	2.0634(18)	Fe1-N1	2.028(4)	Fe1-N1	2.047(2)
S1-Fe1-Cl1	103.77(3)	S2-Fe1-Br1	102.50(4)	S1-Fe1-I1	100.95(3)
S1-Fe1-S2	78.99(3)	S2-Fe1-S1	79.19(5)	S1-Fe1-S2	79.85(3)
S2-Fe1-Cl1	116.44(3)	S1-Fe1-Br1	115.45(4)	S2-Fe1-I1	114.69(3)
N2-Fe1-Cl1	95.78(6)	N2-Fe1-Br1	101.92(10)	N2-Fe1-I1	96.48(8)
N2-Fe1-S1	160.40(6)	N2-Fe1-S2	97.15(11)	N2-Fe1-S1	162.54(8)
N2-Fe1-S2	91.21(6)	N2-Fe1-S1	142.42(11)	N2-Fe1-S2	92.15(8)
N2-Fe1-N1	80.03(7)	N1-Fe1-N2	79.94(15)	N2-Fe1-N1	80.29(10)
N1-Fe1-Cl1	102.60(5)	N1-Fe1-Br1	96.04(11)	N1-Fe1-I1	100.08(7)
N1-Fe1-S1	96.78(5)	N1-Fe1-S2	161.42(11)	N1-Fe1-S2	145.08(8)
N1-Fe1-S2	140.69(6)	N1-Fe1-S1	91.88(12)	N1-Fe1-S1	97.36(7)

a) in M. A. Kopf, D. Varech, J. P. Tuchagues, D. Mansuy, I. Artaud, *J. Chem. Soc., Dalton Trans.* 1998, 991-998.

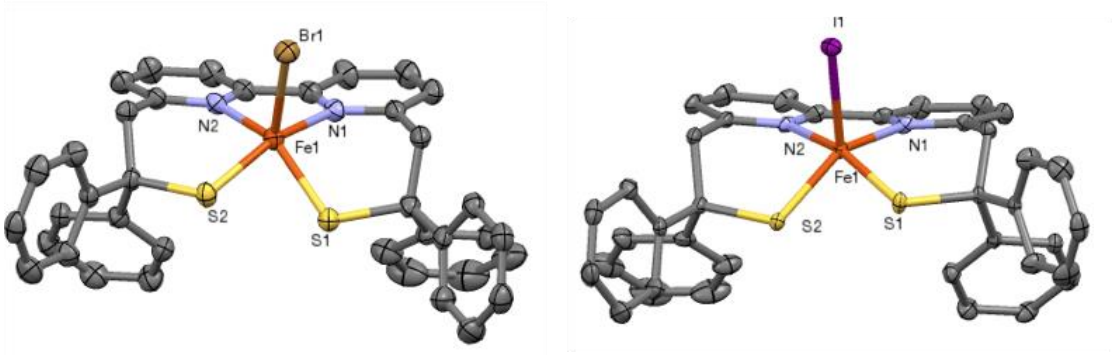

Figure S1.1. Crystal structure of **Fe(L)Br** and **Fe(L)I**. The thermal ellipsoids are drawn at 30% probability level. All hydrogen atoms are omitted for clarity.

S2: Spectroscopic data

Cw-X-band electron paramagnetic resonance (EPR) spectra were recorded with a Bruker EMX, equipped with an Oxford Instruments ESR-900 continuous-flow helium cryostat and an ER-4116 DM Bruker cavity for the 4.5 K experiments. Cw-Q-band EPR spectra were recorded on the same spectrometer equipped with an ER-5106 QTW Bruker cavity. All spectra were recorded at 7K on powder samples.

Mössbauer spectra were recorded with a ^{57}Co source in a Rh matrix using an alternating constant acceleration Wissel Mössbauer spectrometer operated in the transmission mode and equipped with a Janis closed-cycle helium cryostat. The isomer shift is given relative to iron metal at ambient temperature. Simulation of the experimental data was performed with the *Mfit* program using Lorentzian line doublets (E. Bill, Max-Planck Institute for Chemical Energy Conversion, Mülheim/Ruhr, Germany. E-mail: eckhard.bill@cec.mpg.de; webpage:

http://www.cec.mpg.de/research/molecular-theory-and-spectroscopy/moessbauer-mcd.html?L=1).

Temperature-dependent magnetic susceptibility measurements were carried out with a *Quantum-Design* MPMS-XL-5 SQUID magnetometer equipped with a 5 Tesla magnet in the range from 2 to 210 K (**Fe(L)Br** and **Fe(L)I**) or 295 K (**Fe(L)Cl**) in a magnetic field of 0.5 T. The polycrystalline samples were contained in a gel bucket, covered with a drop of low viscosity perfluoropolyether based inert oil Fomblin Y45 to fix the crystals (for **Fe(L)Br** and **Fe(L)I**), and fixed in a non-magnetic sample holder. The maximum measuring temperature of 210 K was chosen because of the pour point of the oil, in order to keep the oil in the frozen state and to avoid therefore the orientation of the crystals parallel to the magnetic field. Each raw data file for the measured magnetic moment was corrected for the diamagnetic contribution of the gel bucket and of the inert oil according to $M^{dia} = \chi_g \cdot m \cdot H$, with experimentally obtained gram susceptibility of gel bucket ($\chi_g = -5.70 \cdot 10^{-7}$ emu/(g·Oe) and of the oil ($\chi_g = -3.8 \cdot 10^{-7}$ emu/(g·Oe)). The molar susceptibility data were corrected for the diamagnetic contribution according to $\chi_M^{dia}(\text{sample}) = -0.5 \cdot M \cdot 10^{-6}$ cm^3·mol^{-1}.

Full-matrix diagonalization of the spin Hamiltonian for zero-field splitting and Zeeman splitting was performed with the *julX_2s* program (E. Bill, Max-Planck Institute for Chemical Energy Conversion, Mülheim/Ruhr, Germany, **2014**). Matrix diagonalization is done with the routine ZHEEV from the LAPACK numerical package. Parameter optimization is performed with the simplex routine AMOEBA from NUMERICAL RECIPES.

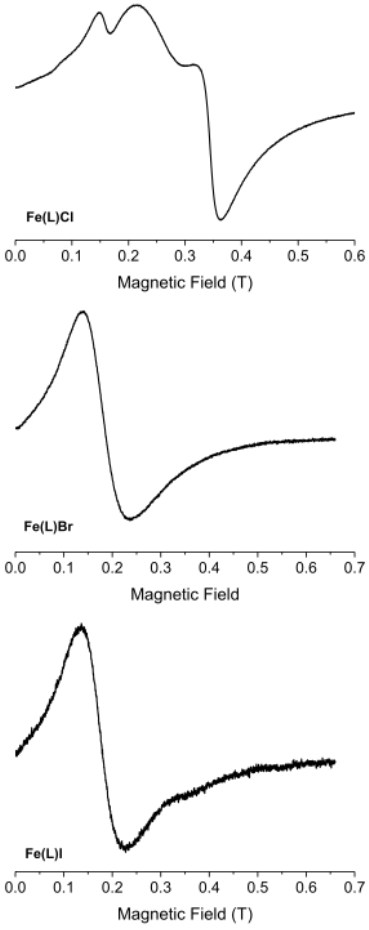

Figure S2.1. X-band EPR spectra.

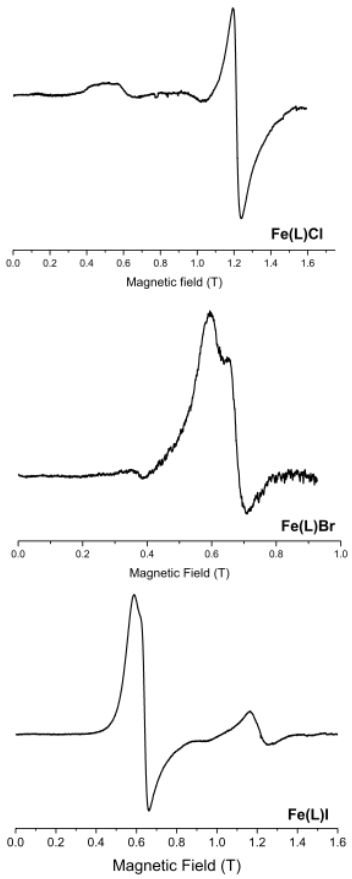

Figure S2.2. Q-band EPR spectra

Analysis of the EPR data. Since the *D* values are large compared to the energy of the both X- and Q- bands (about 0.3 cm^{-1} and 1.2 cm^{-1}, respectively), two different approaches can be used.

The first is related to the determination of the g_{eff} values considering each Kramers doublet as an S= ½ and then to estimate the *E/D* ratio from rhombograms that have been calculated for isotropic g=2 species. The second is to consider the full Hamiltonian with the Zeeman and zero field splitting terms (Eq(1) in the main text) for an S=3/2 species. In this last case, *D* is set to a very large value in such a manner that the spectrum is only affected by varying the *E/*D ratio but not *D*. For the Q-band spectra, estimated values of *D* determined by SQUID and/or predicted by DFT calculations have been also used to confirm the estimated E/D values (since at this frequency, the D value is less large compare at the X-band).

Fe(L)Cl: For this complex, at X-band the g_{eff} values are at 4.6 and 2.7. The resonance at g=2 is attributed to the third g_{eff} contaminated by an isotropic g=2 values (as confirmed at Q-band). From these two g_{eff} values an *E/D* of about 0.18 can be estimated from the rhombogram. At Q-band the g_{eff} values are at 5.4 and 4.0. In this case the rhombogram can not be used any more, illustrating the limitation of this approach (for isotropic g=2 species).

Fe(L)Br and **Fe(L)I**: At X-band the resolution of the spectrum is very bad and only one large resonance can be observed. Our approach was to use the S=3/2 approach with the full spin Hamiltonian and to find a set of parameter with the same *E/D* values and g-values that simulate both spectra. At this point, it is really important to determine a set of parameters that can simulate the spectra recorded at two frequencies since there are four parameters (*E*, and *g*-values) that can be varied (and only one large transition at X-band and two transitions at Q-band).

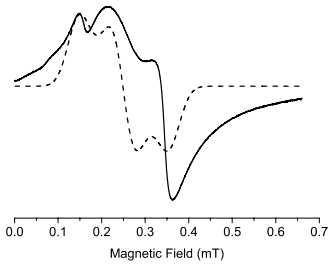

Figure S2.3. Simulated (dashed line) and experimental (bold line) powder EPR X-spectra of **Fe(L)Cl**. Parameters used for the simulation with S= ½ with g_{eff} approach, g_1= 4.6, g_2= 2.7, g_1= 1.9.

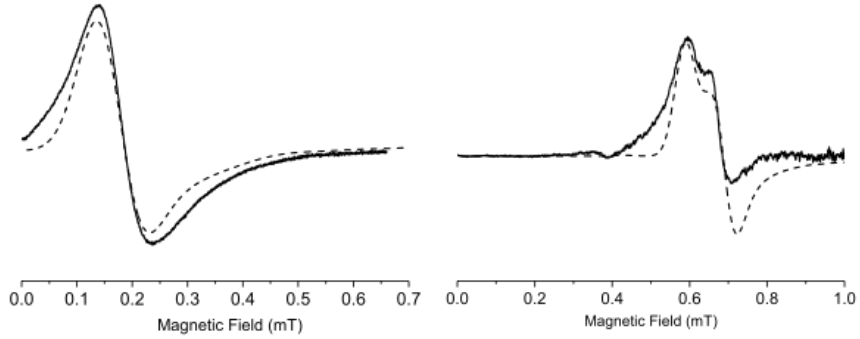

Figure S2.4. Simulated (dashed line) and experimental (bold line) powder EPR X- (left) and Q- (right)-band spectra of **Fe(L)Br**. Parameters used for the simulation with the S= 3/2 approach; g_1= 2.3, g_2= 1.9, g_1= 2.0 and E/D = 0.13.

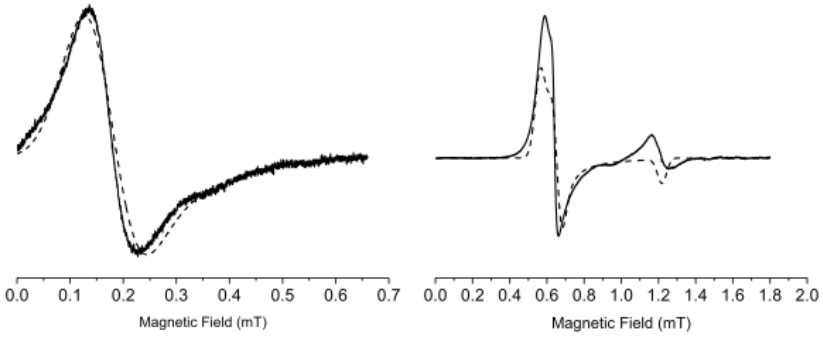

Figure S2.5. Simulated (dashed line) and experimental (bold line) powder EPR X- (left) and Q- (right)-band spectra of **Fe(L)I**. Parameters used for the simulation; g_1= 2.23 g_2= 1.9, g_1= 2.0 and E/D = 0.12.

S3: Spin-state energetics

For investigation of spin state energetics Density Functional Theory (DFT)[1, 2] calculations were carried out, using Amsterdam Density Functional program package (ADF2016)[3, 4]. In first step geometry optimizations were performed using two general gradient approximations (GGA) in the form of OPBE[5] and S12g[6]. Scalar relativistic corrections have been included self-consistently in all calculations by using the

zeroth-order regular approximation (ZORA)[7, 8]. We performed optimizations of all spin states for three complexes under investigation, by letting the structure of each spin state separately relax towards its own equilibrium geometry. We have used spin projection techniques[9] (both for the energy and the gradients) to correct the spin contamination and to obtain the results for the pure doublet state. Molecular orbitals were expanded in an uncontracted set of Slater type orbitals (STOs) of triple-zeta quality with two polarization function (TZ2P)[10, 11]full electron basis set. All calculations were done in a spin-unrestricted restricted fashion. For all calculations two different Becke grid were used (good and very good), in order to investigate the grid influence on relative energy of different spin states.

If we take a look at the relative spin state energetics of optimized structures (Table 1 and Table S3.1) we can clearly see that the grid choice have no influence on the obtained results in the case of OPBE functional. S12g is a relatively new functional and its good performance for both geometry optimizations and spin state energetics is well known, but unlike OPBE, this functional is grid dependent, and we can see the change of the first excited state in the case of **Fe(L)Br**. If we use Becke greed of good quality the first excited state is sextet, but if we use Becke greed of very good quality (and improve the accuracy of the calculation) the first excited state becomes quartet, and this result is in agreement with OPBE. This is not unusual and we need to take into account that both possible excited states are close in energy (less than 2 kcal mol^{-1}).
Furthermore, we performed single point calculations on the crystal structure of examined **Fe(L)X** species. In this regard, we also investigated the influence of spin contamination in the case of doublet spin state. Single point calculations with both functionals showed no grid dependency and confirmed the quartet state as the ground state. Spin contamination showed stabilization effect on the doublet state, and lowered the energy barrier for the excitation. Single point calculations were also carried out in ORCA program package in order to see difference between Slater and Gaussian type orbitals, which showed consistency.

Table S3.1 Spin state energetics obtained by optimization of **Fe(L)Cl**, **Fe(L)Br** and **Fe(L)I**, by carrying out single point calculations on the crystal structure of **Fe(L)Cl**, **Fe(L)Br** and **Fe(L)I**

		Fe(L)Cl	**Fe(L)Br**	**Fe(L)I**
Spin state energetics of **Fe(L)X** relative to ground intermediate spin state, with corrected spin contamination of LS**				
OPBE/TZ2P/ good grid	LS*	7.6	7.5	6.5
	IS*	0.0	0.0	0.0
	HS*	5.5	6.4	7.6
S12g/TZ2P/ good grid	LS	8.3	8.2	7.0
	IS	0.0	0.0	0.0
	HS	7.8	8.5	9.3
Single point calculations carried out on crystal structures of **Fe(L)X,** with corrected spin contamination of LS**				
OPBE/TZ2P/ good grid	LS	16.8	16.0	13.6
	IS	0.0	0.0	0.0
	HS	14.4	15.0	16.6
S12g/TZ2P/ good grid	LS	13.8	12.9	10.5
	IS	0.0	0.0	0.0
	HS	16.4	17.0	18.6
Single point calculations carried out on crystal structures of **Fe(L)X,** without corrected spin contamination of LS				
OPBE/TZ2P/ good grid	LS	13.6	13.0	11.3
	IS	0.0	0.0	0.0
	HS	14.4	15.0	16.6
S12g/TZ2P/ good grid	LS	11.2	10.5	8.9
	IS	0.0	0.0	0.0
	HS	16.4	17.0	18.6
Single point calculations carried out on crystal structures of **Fe(L)X,** with corrected spin contamination of LS**				
OPBE/TZ2P/ very good grid	LS	16.8	16.0	13.5
	IS	0.0	0.0	0.0
	HS	14.4	15.0	16.6
	LS	13.7	12.9	10.5

S12g/TZ2P/ very good grid	IS	0.0	0.0	0.0
	HS	16.4	17.0	18.6

Single point calculations carried out on crystal structures of **Fe(L)X,** without corrected spin contamination of LS

	LS	13.6	13.0	11.3
OPBE/TZ2P/ very good grid	IS	0.0	0.0	0.0
	HS	14.4	15.0	16.6
	LS	11.2	10.6	8.8
S12g/TZ2P/ very good grid	IS	0.0	0.0	0.0
	HS	16.4	17.0	18.6

Single point calculations with Gaussian type orbitals, carried out on crystal structures of **Fe(L)X,** without corrected spin contamination of LS

	LS	13.2	12.7	10.9
OPBE/ZORA-def2-TZVPP	IS	0.0	0.0	0.0
	HS	14.7	15.4	17.0

*LS- low spin, IS- intermediate spin, HS- high spin

**We have used spin projection techniques (both for the energy and the gradients) to correct the spin contamination [http://pubs.acs.org/doi/abs/10.1021/jp0441442] and to obtain the results for the pure doublet state

Table S3.2 Selected bond lengths (Å) obtained from DFT energy-minimized structures for **Fe(L)Cl**, **Fe(L)Br** and **Fe(L)I**

		Fe(L)Cl	Fe(L)Br	Fe(L)I
OPBE/TZ2P/ very good grid	Cl1-Fe1	2.2624	2.4289	2.4289
	Fe1-S1	2.1616	2.1588	2.1588
	Fe1-S2	2.1654	2.1575	2.1575
	Fe1-N2	2.0097	2.0061	2.0061
	Fe1-N1	2.0095	2.0052	2.0052
	LE	0.065	0.066	0.244
	MAE	0.046	0.040	0.068
	RMSE	0.021	0.019	0.043
S12g/TZ2P/ very good grid	Cl1-Fe1	2.2766	2.4432	2.6741
	Fe1-S1	2.1815	2.1775	2.1724
	Fe1-S2	2.1840	2.1780	2.1719
	Fe1-N2	2.0355	2.0320	2.0269
	Fe1-N1	2.0363	2.0311	2.0260
	LE	0.046	0.046	0.038
	MAE	0.028	0.024	0.016
	RMSE	0.013	0.012	0.009

LE- Larges error
MAE- Mean Absolute Error
RMSE- Root Mean Squared Error

1. Koch, W.and Holthausen, M. C., *A Chemist's Guide to Density Functional Theory*. Wiley: 2015.
2. Parr, R. G.and Weitao, Y., *Density-Functional Theory of Atoms and Molecules*. Oxford University Press: 1994.
3. te Velde, G.,Bickelhaupt, F. M.,Baerends, E. J.,Fonseca Guerra, C.,van Gisbergen, S. J. A.,Snijders, J. G.and Ziegler, T. *Journal of Computational Chemistry* **2001,** *22*, 931-967.
4. Pye, C. C.and Ziegler, T. *Theoretical Chemistry Accounts* **1999,** *10*.
5. Klamt, A. *The Journal of Physical Chemistry* **1995,** *99*, 2224-2235.
6. Swart, M. *Chemical Physics Letters* **2013,** *580*, 166-171.
7. Lenthe, E. v.,Ehlers, A.and Baerends, E.-J. *The Journal of Chemical Physics* **1999,** *110*, 8943-8953.
8. Lenthe, E. v.,Baerends, E. J.and Snijders, J. G. *The Journal of Chemical Physics* **1994,** *101*, 9783-9792.
9. Groenhof, A. R.,Swart, M.,Ehlers, A. W.and Lammertsma, K. *The Journal of Physical Chemistry A* **2005,** *109*, 3411-3417.
10. Van Lenthe, E.and Baerends, E. J. *Journal of Computational Chemistry* **2003,** *24*, 1142-1156.
11. Chong, D. P.,Van Lenthe, E.,Van Gisbergen, S.and Baerends, E. J. *Journal of Computational Chemistry* **2004,** *25*, 1030-1036.

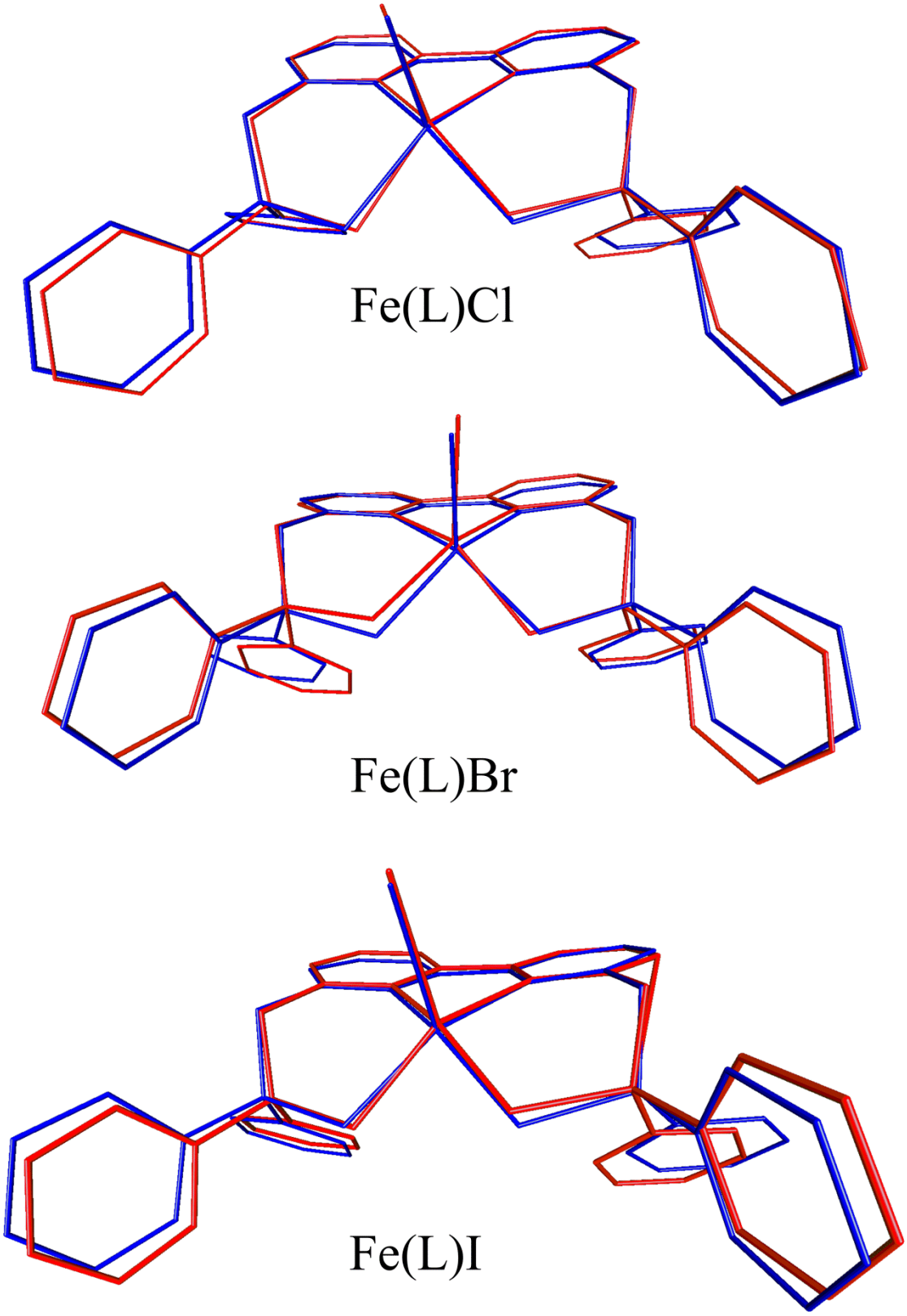

Figure S3.1 Overlap of crystal (red) and S12g optimized structures (blue) of **Fe(L)X** (X=Cl, Br, I)

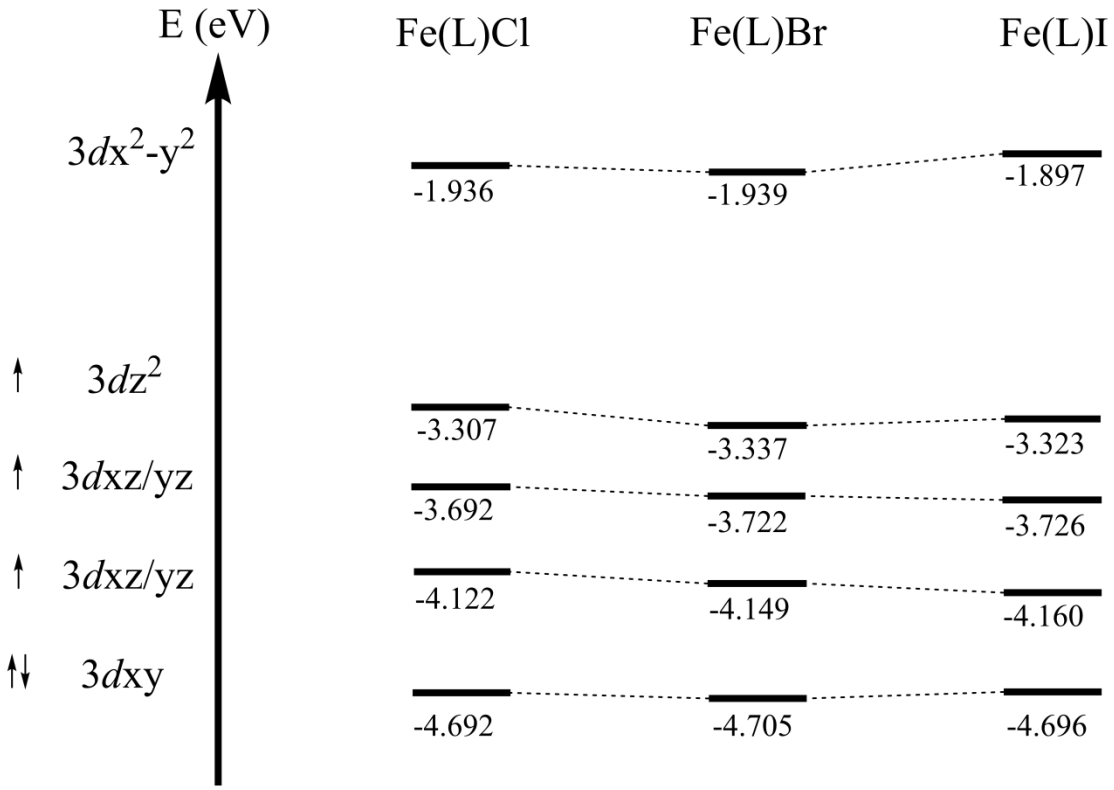

Figure S3.2 Energy levels of five *d* orbitals in **Fe(L)X** (X=Cl, Br, I)

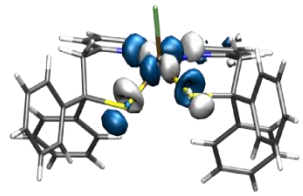

$d_{x^2-y^2}$ - σ-antibonding

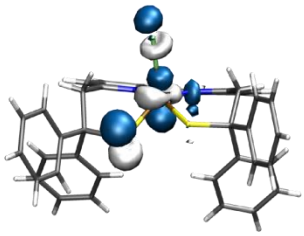

d_{z^2} - σ/π-antibonding

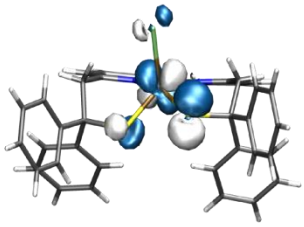

d_{yz}/d_{xz} - π-antibonding

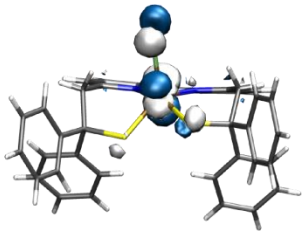

d_{xz}/d_{yz} - π-antibonding

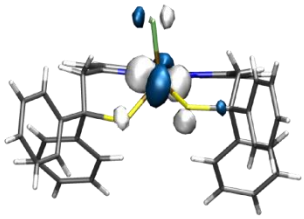

d_{xy} - non-bonding

Figure S3.3 Kohn-Sham molecular orbitals with dominant metal *d* character for **Fe(L)X**, X=Cl

S4: Zero Field Splitting calculations

Zero Field Splitting (ZFS) parameters were obtained from relativistic single-point calculations on the experimentally determined X-ray structures with ORCA program package (version 4.0.1.2)[1]. Scalar relativistic effects were considered at the Zero-Order-Regular-Approximation (ZORA)[2] level. Picture change effects were taken into account. Spin−orbit coupling was included in the mean-field approximation (SOMF), with both the spin-own-orbit and spin-other-orbit interactions in the exchange term, as well as with the coupled-perturbed (CP)[3] approach. The spin−spin contribution was calculated using a restricted spin-density obtained from singly occupied unrestricted natural orbitals (uno)[4]. Since the predicted ZFS values are highly sensitive to the level of theory employed, we explored different density functional approximations (OLYP[5, 6, 7], BP86[8, 9], OPBE[10, 11] and TPSS[12]) and basis sets (ZORA-def2-TZVP and ZORA-def2-TZVPP).[13, 14] For iodine atom old-ZORA-TZVPP basis set was used. The resolution of the identity (RI) approximation[15] in the Split-RI-J variant with the scalar relativistically recontracted SARC/J[14, 16, 17] Coulomb fitting sets has been used. In the main text, results at BP86/ ZORA-def2-TZVP level of theory are given.

Table S4.1. CP-DFT calculated ZFS parameters of **Fe(L)Cl**, **Fe(L)Br** and **Fe(L)I** at different levels of theory*

		Fe(L)Cl	**Fe(L)Br**	**Fe(L)I**
OLYP/ZORA-def2-TZVP	D (cm^{-1})	2.24	4.40	9.83
	E/D	0.12	0.03	0.31
	D_{SSC} (cm^{-1})	0.29	0.16	0.00
	D_{SOC} (cm^{-1})	1.95	4.24	9.83
OLYP/ZORA-def2-TZVPP	D (cm^{-1})	2.23	4.35	9.62
	E/D	0.13	0.03	0.31
	D_{SSC} (cm^{-1})	0.29	0.16	0.00
	D_{SOC} (cm^{-1})	1.94	4.18	9.62
OPBE/ZORA-def2-TZVP	D (cm^{-1})	2.24	4.56	-8.50
	E/D	0.11	0.02	0.32
	D_{SSC} (cm^{-1})	0.30	0.17	0.05
	D_{SOC} (cm^{-1})	1.93	4.39	-8.54
OPBE/ZORA-def2-TZVPP	D (cm^{-1})	2.22	4.50	-8.31
	E/D	0.12	0.03	0.32
	D_{SSC} (cm^{-1})	0.31	0.17	0.04
	D_{SOC} (cm^{-1})	1.92	4.32	-8.35
BP86/ZORA-def2-TZVP	D (cm^{-1})	2.34	4.72	12.42
	E/D	0.17	0.06	0.32
	D_{SSC} (cm^{-1})	0.26	0.13	0.00
	D_{SOC} (cm^{-1})	2.08	4.59	12.42
BP86/ZORA-def2-TZVPP	D (cm^{-1})	2.33	4.66	12.30
	E/D	0.18	0.06	0.33

	D_{SSC} (cm^{-1})	0.26	0.13	0.00
	D_{SOC} (cm^{-1})	2.07	4.52	12.30
TPSS/ZORA-def2-TZVP	D (cm^{-1})	2.00	3.57	9.50
	E/D	0.27	0.09	0.32
	D_{SSC} (cm^{-1})	0.26	0.11	0.04
	D_{SOC} (cm^{-1})	1.73	3.46	9.46
TPSS/ZORA-def2-TZVPP	D (cm^{-1})	1.99	3.51	9.24
	E/D	0.27	0.09	0.32
	D_{SSC} (cm^{-1})	0.26	0.11	0.05
	D_{SOC} (cm^{-1})	1.95	3.40	9.19

*Basis set for iodine is always old-ZORA-TZVPP.

As it can be seen from Table S4.1, the influence of basis set is very small. This is particularly for chloride complex, where ZFS parameters are essentially the same. For iodide complex difference is up to 0.2 cm^{-1}. Density functional approximation employed is more important. For chloride and bromide complexes values for *D* are consistent and go from around 2.0-2.3 and 3.5-4.7, respectively, depending on the employed functional. TPSS is underestimating *D* values, while OLYP and OPBE are giving very similar results in these complexes. However, for Iodide complex OPBE gives right order of magnitude for *D* value but with opposite sign, comparing to other, GGA (OLYP and BP86) or metaGGA (TPSS) functionals, and to the experimental findings. *E/D* values for iodide complex has been calculated to be large, coming close to the rhombic limit of 1/3 where the sign of *D* is ambiguous.

Another method used for the calculation of ZFS parameters is the ligand-field DFT (LF-DFT) approach by C. Daul et al.[18, 19], based on a multideterminant description of the transition metal's multiplet fine structure. It works by evaluating the DFT energy of all the Slater determinants arising from the d^n configuration (252 Slater determinants for the case of d^5 configuration) of the transition-metal ion in the environment of coordinating ligands using Kohn−Sham (KS) orbitals. The orbitals are generated in an average of configuration (AOC) spin-restricted calculation with all *d* electrons distributed evenly over the five KS molecular orbitals dominated by *d* orbitals. This set of energies is then analyzed within a ligand-field model to obtain variationally the energy and multideterminant wave function of the ground and excited states. With this procedure we can calculate all customary molecular properties, aware that its validity decreases with increasing metal−ligand covalency. Details about the LF-DFT procedure can be found elsewhere[20]. Calculations were carried out on the experimentally determined X-ray structures using the Amsterdam Density Functional (ADF) code at ZORA OPBE/TZP level of theory, proven to be method of choice for LF-DFT. A comparison between the energies of all the SD calculated by DFT and by LF parametrization shows an excellent quality of the fit (the mean square deviation between the two sets of energies, *msd* is between 100-106 cm^{-1}). Non-empirically determined Racah's parameters (*B* and *C*) and orbital reduction factor (*orf*) for all three complexes are given in Table S4.2, while splitting of KS molecular orbitals is given in Figure S3.2, and orbitals are depicted in Figure S3.3. It is obvious that all three complexes are very covalent, and covalency increases, but only slightly going from chloride to iodide complex. Therefore, covalency is largely governed by L^{N2S2} (sulphur ligators).

Intermediate ground state is a consequence of strong and covalent bonding in *xy* plane, and weak bonding between metal and axial ligand. Consequently, d_{x2-y2} orbital is highest in energy, and separated from other four metal based orbitals, including d_{z2} orbital. At the

same time, nephelauxetic reduction due to the covalency lowers pairing energy, leading to the pairing of two electrons in mainly non-bonding d_{xy} orbital and intermediate ground spin-state.

Table S4.2. Non-empirically determined ligand-fied parameters of **Fe(L)Cl**, **Fe(L)Br** and **Fe(L)I** obtained by LF-DFT procedure and energies of lowest lying electronic states with different multiplicities (in kcal/mol)

	Fe(L)Cl	**Fe(L)Br**	**Fe(L)I**
B (cm^{-1})	236	229	236
C (cm^{-1})	2626	2627	2496
orf	0.65	0.64	0.63
msc (cm^{-1})	102	106	100
IS (S=3/2)	0.0	0.0	0.0
HS (S=5/2)	11.5	12.0	14.9
LS (S=1/2)	11.6	11.7	9.6

Energies of lowest lying excited states with different multiplicities (Table S4.2) are in qualitative agreement with single point calculations carried out with standard DFT (Table S3.1), intermediate spin being ground state, with sextet and doublet states being close in energy in chloride and bromide complex, while doublet being lowest excited state in iodide complex. The order of excited states is related to the increased covalency when going to complexes with heavier halides. For iodide complex there is a dramatic reduction of the parameter C, Table S4.1, leading to the stabilization of the LS excited state.

Furthermore, we have used LF-DFT to calculate ZFS parameters of the complexes, and to compare it with CP-DFT results and experiment. Spin–orbit coupling constant, needed to obtain ZFS parameters, was deduced for chloride complex from the least square fit of the energy splitting of the spinors, obtained by the relativistic ZORA spin–orbit DFT calculations, to the one-electron ligand field model, Table S4.3. Unfortunately, one-electron ligand-field model was unable to reproduce spin-orbit splitting in bromide and iodide complexes. This is because influence of the spin-orbit of heavy halide ligands cannot be treated by ligand-field theory, invalidating the basic approximations of LF-DFT. ZFS parameters of chloride complex were deduced using an effective Hamiltonian approach from the lowest eigenvalues and corresponding eigenvectors from LF-DFT multiplet calculations, in the basis of ±1/2 and ±3/2 M_S wave functions. Results for the chloride complex are given in Table S4.3. Calculated ZFS parameters are in excellent agreement with both experiment (*D*=3.7, *E/D*=0.18) and CP-DFT (Table S4.1). In addition, LF-DFT shows that doublet exited states are most important for both the magnitude and sign of *D* value, as predicted by CP-DFT (see the main text).

Unfortunately, one-electron ligand-field model was unable to reproduce spin-orbit splitting in bromide and iodide complexes. Although this may look surprising on the first sight, this is a consequence of increased covalency in a series, that causes diminishing importance of the metal spin-orbit coupling. Following only this trend of increasing covalency, and staying in the framework of standard ligand field theory with a single (metal ion based) spin-orbit constant, one may expect lowering of ZFS, contrary to what is observed. However, at the same time, more covalent character of metal-halide bond, implies that importance of the spin-orbit contribution of the heavier halides cannot be neglected. Influence of the spin-orbit of heavy halide ligands cannot be treated by the ligand-field theory which assumes a single (metal ion based) spin-orbit constant. Therefore, the basic approximations of LF-DFT are not valid in the cases of bromide and iodide complexes. Nevertheless, large covalent character of metal-ligand bonds, makes CP-DFT well suited for analysis of the ZFS in these

systems, as seen from a good agreement with experimental values (see the main text and Table S4.1).

Table S4.3. LF-DFT calculated ZFS Parameters of **Fe(L)Cl** and decomposition of *D* parameter into contributions from the excited states with different multiplicities.

	Fe(L)Cl
D(cm^{-1})	2.6
E/D	0.1
Zeta (cm^{-1})	199
D_{SOC} (S=3/2) (cm^{-1})	0.23
D_{SOC} (S=1/2) (cm^{-1})	3.21
D_{SOC} (S=5/2) (cm^{-1})	-0.79

1. Neese, F. *Wiley Interdisciplinary Reviews: Computational Molecular Science* **2012,** *2*, 73-78.
2. Wüllen, C. v. *The Journal of Chemical Physics* **1998,** *109*, 392-399.
3. Neese, F.and Solomon, E. I. *Inorganic Chemistry* **1998,** *37*, 6568-6582.
4. Hirata, S.and Head-Gordon, M. *Chemical Physics Letters* **1999,** *302*, 375-382.
5. Handy, N. C.and Cohen, A. J. *Molecular Physics* **2001,** *99*, 403-412.
6. Hoe, W.-M.,Cohen, A. J.and Handy, N. C. *Chemical Physics Letters* **2001,** *341*, 319-328.
7. Lee, C.,Yang, W.and Parr, R. G. *Physical Review B* **1988,** *37*, 785-789.
8. Becke, A. D. *Physical Review A* **1988,** *38*, 3098-3100.
9. Perdew, J. P. *Physical Review B* **1986,** *33*, 8822-8824; Perdew, J. P. *Physical Review B* **1986,** *34*, 7406-7406.
10. Perdew, J. P.,Burke, K.and Ernzerhof, M. *Physical Review Letters* **1996,** *77*, 3865-3868.
11. Swart, M.,Ehlers, A. W.and Lammertsma, K. *Molecular Physics* **2004,** *102*, 2467-2474.
12. Tao, J.,Perdew, J. P.,Staroverov, V. N.and Scuseria, G. E. *Physical Review Letters* **2003,** *91*, 146401.
13. Weigend, F.and Ahlrichs, R. *Physical Chemistry Chemical Physics* **2005,** *7*, 3297-3305.
14. Pantazis, D. A.,Chen, X.-Y.,Landis, C. R.and Neese, F. *Journal of Chemical Theory and Computation* **2008,** *4*, 908-919.
15. Neese, F. *The Journal of Chemical Physics* **2001,** *115*, 11080-11096.
16. Pantazis, D. A.and Neese, F. *Journal of Chemical Theory and Computation* **2009,** *5*, 2229-2238.
17. Weigend, F. *Physical Chemistry Chemical Physics* **2006,** *8*, 1057-1065.
18. Atanasov, M.and Daul, C. A. *Chemical Physics Letters* **2003,** *381*, 584-591.
19. Atanasov, M.,Daul, C. A.and Rauzy, C., In *Optical Spectra and Chemical Bonding in Inorganic Compounds*, Mingos, D. M. P.; Schönherr, T., Eds. Springer: Berlin, Heidelberg, 2004; Vol. 106, pp 97–125.
20. Perić, M.,García-Fuente, A.,Zlatar, M.,Daul, C.,Stepanović, S.,García-Fernández, P.and Gruden-Pavlović, M. *Chemistry – A European Journal* **2015,** *21*, 3716-3726.